Article

Synthesis of Electron-Rich Porous Organic Polymers via Schiff-Base Chemistry for Efficient Iodine Capture

Peng Tian [1,†], Zhiting Ai [1,†], Hui Hu [1], Ming Wang [1], Yaling Li [1], Xinpei Gao [1], Jiaying Qian [1], Xiaofang Su [1,*], Songtao Xiao [2,*], Huanjun Xu [3], Fei Lu [1] and Yanan Gao [1,*]

[1] Key Laboratory of Ministry of Education for Advanced Materials in Tropical Island Resources, Department of Chemistry and Chemical Engineering, Hainan University, No 58, Renmin Avenue, Haikou 570228, China
[2] China Institute of Atomic Energy, Beijing 102413, China
[3] School of Science, Qiongtai Normal University, Haikou 571127, China
* Correspondence: sxf@hainanu.edu.cn (X.S.); xiao200112@163.com (S.X.); ygao@hainanu.edu.cn (Y.G.)
† These authors contributed equally to this work.

Abstract: As one of the main nuclear wastes generated in the process of nuclear fission, radioactive iodine has attracted worldwide attention due to its harm to public safety and environmental pollution. Therefore, it is of crucial importance to develop materials that can rapidly and efficiently capture radioactive iodine. Herein, we report the construction of three electron-rich porous organic polymers (POPs), denoted as POP-E, POP-T and POP-P via Schiff base polycondensations reactions between *Td*-symmetric adamantane knot and four-branched "linkage" molecules. We demonstrated that all the three POPs showed high iodine adsorption capability, among which the adsorption capacity of POP-T for iodine vapor reached up to 3.94 $g \cdot g^{-1}$ and the removal rate of iodine in n-hexane solution was up to 99%. The efficient iodine capture mechanism of the POP-T was investigated through systematic comparison of Fourier transform infrared spectroscopy (FT-IR), Raman spectroscopy and X-ray photoelectron spectroscopy (XPS) before and after iodine adsorption. The unique π-π conjugated system between imine bonds linked aromatic rings with iodine result in charge-transfer complexes, which explains the exceptional iodine capture capacity. Additionally, the introduction of heteroatoms into the framework would also enhance the iodine adsorption capability of POPs. Good retention behavior and recycling capacity were also observed for the POPs.

Keywords: porous organic polymers; iodine capture; radioiodine; electron-rich framework; charge-transfer complexes

1. Introduction

Nuclear energy, as a clean energy source, has become one of the most realistic alternative energy sources in society today. The use of nuclear energy to generate electricity would greatly reduce carbon dioxide emissions, which will help alleviate the growing greenhouse effect of global warming. Nuclear energy is playing an increasingly important role in current energy supply due to its ultra-high energy density and low carbon emissions. However, the large amount of nuclear waste generated in the process of nuclear fission has seriously affected the environment and human health. So, how to deal with these nuclear wastes safely and efficiently is an urgent problem to be solved [1,2]. Radioactive iodine ([129]I and ^{131}I) is one of the main nuclear wastes and is also considered to be a radioactive pollutant in nuclear power plants. [129]I must be trapped and stored timely at disintegration because it has an exceptionally long half-live of 15.7 million years. Whereas ^{131}I has a short lifetime of about 8 days, it needs to be immediately captured because of its highly mobile and volatile characteristics [3,4]. Therefore, it has become imperative to develop stable and effective methods for capture and storage of radioiodine.

To this end, various porous materials have been attempted for radioiodine capture. For example, inorganic porous materials such as activated carbon [5–7], zeolites [8–10] and silver-functionalized silica aerogels [11–13] have been used as adsorbents to capture radioiodine. However, these materials usually exhibit low absorption capacity due to their limited surface area and less interactive sites with iodine. Although metal-organic frameworks (MOFs) generally possess high surface area, their low absorption capacity and instability towards moisture has limited the practical applications [14–17]. In recent years, porous organic polymers (POPs) have also attracted a lot of attention for worthwhile iodine capture. POPs are a class of multi-dimensional porous organic materials, which are constructed via strong covalent linkages between various organic building units with different geometries and topologies. Depending on the degree of long-range order, POPs can be divided into amorphous materials, such as conjugated microporous polymers (CMPs) [18–22], porous aromatic frameworks (PAFs) [23–26], hyper-crosslinked polymers (HCPs) [27–29] and crystalline materials, including covalent triazine frameworks (CTFs) [30–33] and covalent organic frameworks (COFs) [34–36]. To date, a large number of COFs have been studied extensively for the capture of iodine and they have showed great potential as adsorbents for the effective removal of radioiodine [37–39]. However, it is known that the synthesis of crystalline COFs remains greatly challenging due to the lack of a universal protocol to guarantee high crystallinity of COFs. In many cases, a great deal of effort has to be expended on screening for optimal reaction conditions. Compared with crystalline COFs, amorphous POPs are much easier to be synthesized since POPs are generally formed via various C–C cross-coupling reactions, such as Suzuki [40,41], Heck [42], Sonogashira [43,44], Yamamoto [45], and Glaser [46] cross-coupling. The formation of C–C bonds are effectively catalysed by metal species and POPs are obtained with a high yield in large quantities. Besides, some POPs are linked to form through the condensation reactions of building units [47]. Therefore, amorphous POPs show better practical application prospects than crystalline COFs.

It is widely accepted that the electron donor character of the porous adsorbent is a critical parameter that will determine the I_2 capture efficiency [48]. Therefore, the affinity and the accessibility of electron donor groups should be modulated when designing POPs framework architectures. Electron-rich structural units can be introduced into the framework, and the electron transfer ability could be enhanced by extending the conjugation of the porous POPs. In this way, it is more beneficial to improve the binding ability of iodine with POPs, so as to achieve the purpose of enhancing the iodine capture ability of POPs.

With these considerations in mind, we successfully synthesized a series of electron-rich POPs (POP-E, POP-T and POP-P), which were constructed through the linkage of imine bonds (Scheme 1). The conjugated π-system and nitrogen atoms in the polymers enabled the strong interactions between the POPs and iodine [49]. Also, the Lewis acid-base interactions between the polar C–N bond and iodine molecules increased the uptake capacity of iodine [50]. In this study, POP-E, POP-T and POP-P showed good efficiency for volatile iodine capture, which could reach 3.49, 3.94 and 3.27 $g \cdot g^{-1}$, respectively. Moreover, the POP absorbents also exhibited great iodine removal ability in iodine-n-hexane solution; for instance, the removal efficiency for POP-T in 500 $mg \cdot L^{-1}$ iodine-n-hexane solution could reach up to 99%.
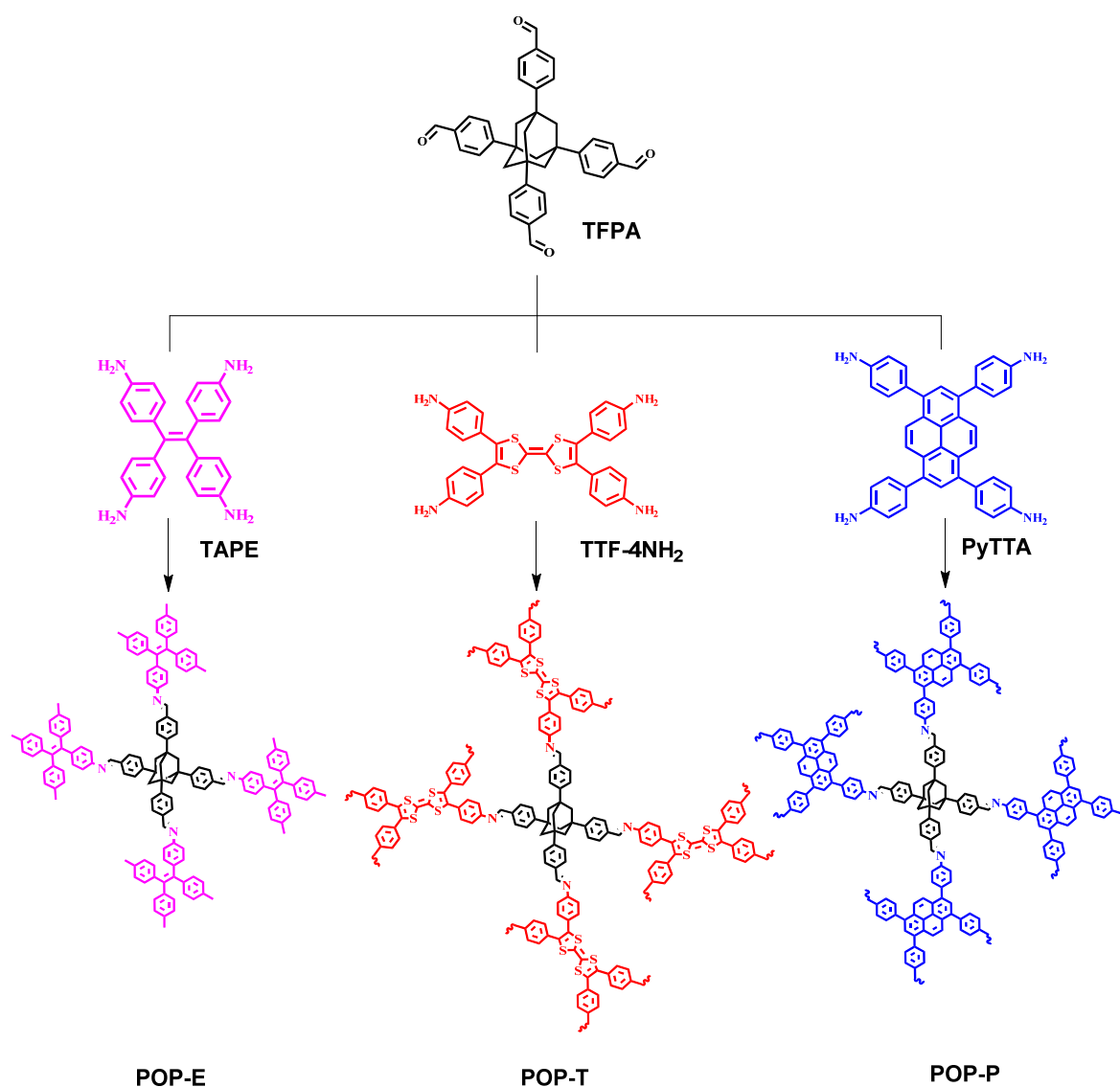
Scheme 1. Structures of POP-E, POP-T, and POP-P.

2. Results and Discussion

The synthesis route of POP-E, POP-T and POP-P was shown in Scheme 1. The three POPs were constructed through the Schiff base condensation reaction in the presence of 1,2-dichlorobenzene and acetic acid at 120 °C. The synthesis details of the monomers and the corresponding ^{1}H NMR results (Figure S1–S7) are given in supporting information (SI). The successful formation of POPs (POP-E, POP-T and POP-P) was confirmed by Fourier transform infrared spectroscopy (FT-IR) using an attenuated total reflection (ATR) mode (Figure 1). For the FT-IR spectra of tetrakis (4-aminophenyl) ethene (TAPE), 4,4′,4″,4‴-([2,2′-bi(1,3-dithiolylidene)]-4,4′,5,5′-tetrayl)tetraaniline (TTF-4NH$_2$) and 1,3,6,8-tetrakis (4-aminophenyl) pyrene (PyTTA) monomers, the absorption bands between 3400 and 3200 cm^{-1} are due to the N-H stretching vibration. The absorption peaks around 1700 cm^{-1} can be ascribed to the -C=O stretching vibration. After the Schiff-base condensation reaction, the absorption bands between 3400 and 3200 cm^{-1} almost disappeared in the FT-IR spectra of POP-E, POP-T and POP-P, indicating a high degree of polymerization between the amine and aldehyde groups of the monomers. Meanwhile, several new absorption peaks appeared after the reaction between the two units. The peaks at 1663 cm^{-1}, 1624 cm^{-1} and 1623 cm^{-1} represented the imine bonds for POP-E, POP-T and POP-P, respectively. It is worth noting that there were still characteristic absorption peaks of the aldehyde group

existing in the three POPs, which suggests incomplete reaction between the amine and aldehyde groups.
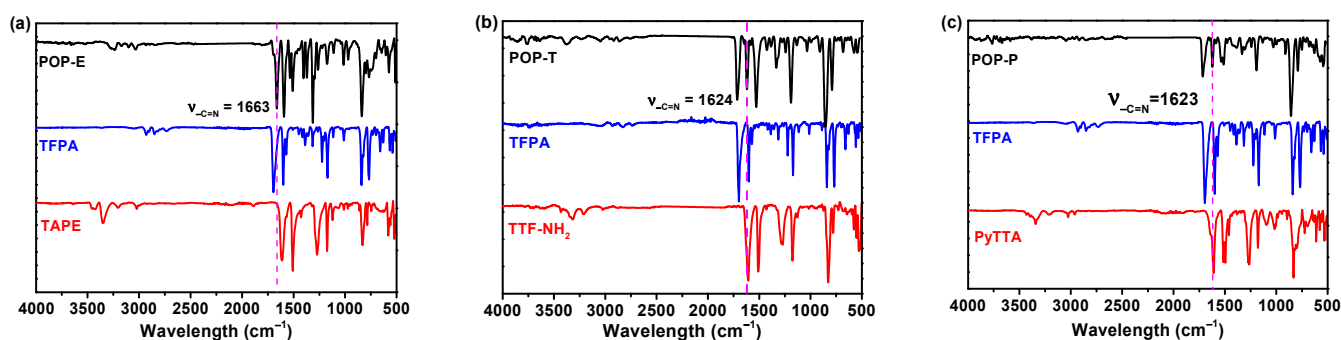

Figure 1. FT-IR spectra of TAPE, TFPA and POP-E (**a**), TTF-NH$_2$, TFPA and POP-T (**b**) and PyTTA, TFPA and POP-P (**c**).

The amorphous structure of POP-E, POP-T and POP-P was confirmed by Powder X-ray diffraction (PXRD), as shown in Figure S8. Thermogravimetric analysis (TGA) was used to test the thermal stability of three POPs under nitrogen conditions and observed that the three POPs are thermal stable up to 200 °C. Furthermore, when the temperature reached 800 °C, there was still 54%, 35% and 45% of the weight retained by POP-E, POP-T and POP-P, respectively, indicating that all three POPs possess good thermal stability (Figure S9). The field-emission scanning electron microscope (FE-SEM) was used to observe the topographic features of the POPs (Figure S10). POP-E exhibited a honeycomb columnar structure. POP-T was mainly formed by disordered the stacking of several nano-spherical particles. POP-P was composed of disordered arrangement of granular solids with nanometric scale.

The nitrogen adsorption−desorption isotherm curves of POP-E, POP-T and POP-P were recorded at 77 K and shown in Figure 2. It can be seen that the nitrogen adsorption and desorption curves of these POPs were similar. When the relative pressure was lower than 0.1 ($P/P_0 < 0.1$), the amount of nitrogen adsorption by the porous materials increased slowly, indicating that there existed microporous structures in the material. When the relative pressure was higher than 0.1 but lower than 0.9 ($0.1 < P/P_0 < 0.9$), the adsorption capacity of the POPs for nitrogen increased slowly; there was a hysteresis loop between the nitrogen adsorption curve and the desorption curve of the material, suggesting the mesoporous nature of the three POP materials. Furthermore, when the relative pressure was in the range from 0.9 to 1.0 ($0.9 < P/P_0 < 1.0$), the nitrogen adsorption by the materials increased sharply, indicating the co-existence of macropore structures in the three POPs. The test results showed that all three POPs possess hierarchical pore structures. The Brunauer–Emmett–Teller (BET) surface areas of POP-E, POP-T and POP-P were calculated as 37.0, 18.3 and 27.8 m^2·g^{-1}, respectively, while the corresponding total pore volume was estimated from single-point nitrogen uptake at $P/P_0 = 0.99$ to be 0.027, 0.037 and 0.058 m^3·g^{-1}, respectively. Finally, the average pore size distribution of POP-E, POP-T and POP-P was calculated to be 1.4, 1.6 and 1.2 nm, respectively, according to nonlocal density functional theory pore size distribution (NLDFT), which indicated that all three POPs were dominated by microporous structures.

After understanding the structures and properties of the three POPs, the iodine vapor adsorption capacity of the POPs was explored. [127]I was used because of its similar chemical properties to radioactive iodine nuclides [48]. A little amount of POP adsorbent and excess iodine were placed into an airtight system at 348 K under ambient pressure. The iodine uptake capacity of the samples was evaluated by calculating the weight changes of the samples before and after iodine vapor adsorption. (Details are given in Section S3 in the Supplementary Materials)
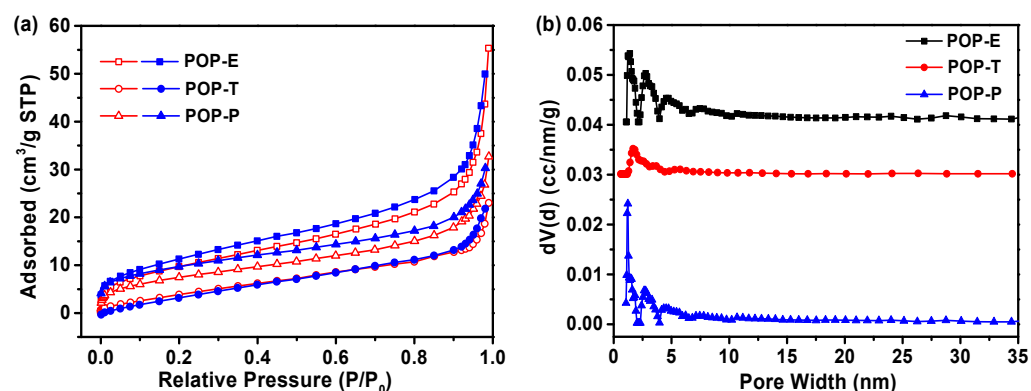
Figure 2. (**a**) Nitrogen adsorption/desorption isotherms of POP-E, POP-T and POP-P. (**b**) Pore size distributions of POP-E, POP-T and POP-P.

It can be seen from the iodine adsorption curve (Figure 3) that the iodine was rapidly adsorbed by POPs at 75 °C within the initial 20 h, which could be attributed to the hierarchical porous structure of the porous material [51]. Among the three POPs, POP-T showed the best iodine vapor uptake ability. After 30 h, the weight growth of the three POPs gradually slowed down, indicating that the adsorption of iodine vapor was close to saturation. Based on these observations, the iodine vapor adsorption experiments of the POPs were continued for another 42 h. It was found that when the adsorption time reached 72 h, the weight of POPs no longer changed obviously, indicating that the iodine uptake of POP-E, POP-T and POP-P was completely saturated. Meanwhile, the colour of the three POPs turned black after the saturated adsorption of iodine, which was related to the deposition of iodine on the surface of the POPs and suggested the high uptake degree of iodine. After calculation, the iodine adsorption capacity of POP-E, POP-T and POP-P was 3.49, 3.94 and 3.27 g·g^{-1}, respectively, indicating that all three POPs have good iodine adsorption capacity.
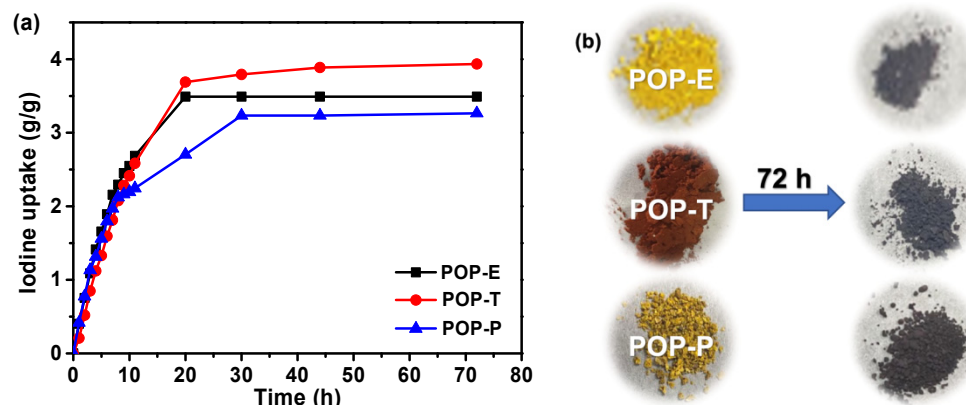

Figure 3. (**a**) Iodine vapor adsorption curves at 75 °C under ambient pressure for POP-E, POP-T and POP-P, (**b**) Colour change of POP samples before and after iodine vapor adsorption.

Compared with reported POPs, it is obvious that POP-E, POP-T and POP-P exhibited outstanding iodine adsorption capacity, better than most other materials (Table S1). Although the BET surface areas of the three POPs was not high, their iodine adsorption capacity was still strong, which shows that the specific surface area and pore volume of iodine adsorbents were not the decisive factors to determine the iodine adsorption performance of POPs. The high iodine capability of the POPs can be ascribed to the introduction of monomers with large π-π conjugated structural units into POPs that could expand the conjugation of the polymer network [37]. Among the three POPs, POP-T showed a better iodine capture performance. The introduction of heteroatoms (sulfer here) with lone pairs of electrons into the electron-rich building blocks could additionally increase the

adsorption of iodine vapor [52]. Specifically, the microporous structure was beneficial for the adsorption of iodine, while the mesoporous and microporous structures were beneficial to the mass transfer process of iodine. These factors could endow POP-T with superior iodine adsorption performance.

To verify the mechanism of iodine adsorption, X-ray photoelectron spectroscopy (XPS) and Raman spectroscopy were used to detect the interaction between the captured iodine and the electron-rich framework of the POP-T. The POP with loaded iodine is referred to as I_2@POP. In the XPS spectra (Figure S11), the N 1s of POP-T showed two binding energy peaks at 399.0 and 400.2 eV, which correspond to C=N and C-N, respectively. After iodine loading, the binding energy of 399.0 eV belonging to C=N slightly shifted to 399.1 eV, while a new peak with binding energy of 401.1 eV appeared. This new peak may have been shifted from 399 eV because of the interactions between lone pairs of electrons on nitrogen atoms and the uptake of electron-deficient iodine. In addition, comparing the Raman spectra of POP-T before and after adsorption of iodine, it could be clearly observed that new absorption peaks at 108 and 165 cm^{-1} were generated (Figure 4a), which could be assigned to the resonant modes of polyiodides, mainly I_3^- and I_5^- anions. The band at 108 cm^{-1} was ascribed to the symmetric and asymmetric stretching vibrations of I_3^- and the peak at 165 cm^{-1} was assigned to the I_5^- stretching vibration [53,54]. Moreover, the existence of polyiodide anions I_3^- and I_5^- was further confirmed by XPS spectra. Two groups of I 3d signals of iodine were observed in the XPS spectrum of I_2@POP-T (Figure 4b). From the XPS spectrum, the I_3^- signal could be observed at 618.2 and 629.8 eV, while the peaks at 619.6 and 631.1 eV were possibly due to the I_5^- signal. As shown in the FTIR spectra (Figure S12), the peak at 1628 cm^{-1} ascribed to C=N blue-shifted to 1641 cm^{-1} while the peak at 1602 cm^{-1} related to C=C red-shifted to 1595 cm^{-1}. Based on the previous reports [37,49] and the above results, it can be concluded that the π-π conjugated systems comprising of the phenyl rings and imine groups should be involved in the formation of charge transfer complex with iodine. As a result, the chemisorption via charge transfer led to the high iodine uptake capacity of POP-T.
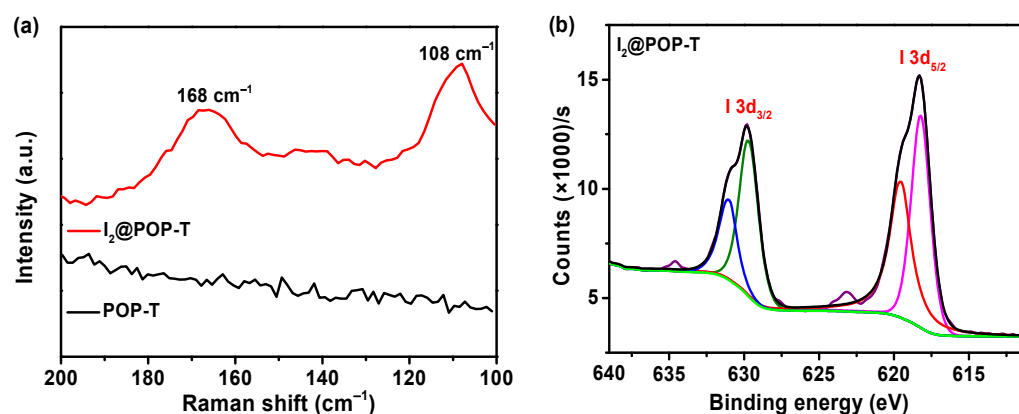

Figure 4. (**a**) Raman spectra of POP-T and I_2@POP-T and (**b**) XPS spectrum of I_2@POP-T.

As an important indicator to assess the performance of porous materials in nuclear industry, the iodine desorption capacity of porous materials is worth studying. Therefore, we investigated the iodine release behavior of I_2@POP-T into methanol. The delivery of iodine from I_2@POP-T into methanol was monitored by using UV/Vis spectroscopy (Figures S13 and S14). It was obvious that about 90% of adsorbed iodine was quickly released within 120 min, displaying the excellent desorption capacity of POP-T (Figure 5a). Also, the retention capacity of iodine captured in the pores of POP-T was also detected. TGA was used to study the retention capacity of I_2@POP-T (Figure S15). The iodine was slowly removed at temperature higher than about 100 °C, suggesting a good retention behavior of POP-T. We can attribute this good retention capacity to strong chemisorption via charge transfer between the framework of the POP and captured iodine. Besides, it is

expected that the absorbent can be cycled for repeated use. The iodine in pores of I_2@POP-T was removed through Soxhlet extraction with methanol for 48 h. After being vacuum-dried at 120 °C for 6 h, samples are reused for iodine vapor absorption. The results showed that POP-T still possessed a high adsorption capacity of 3.2 g·g^{-1} after the fifth recycling, suggesting a good recyclability (Figure 5b).
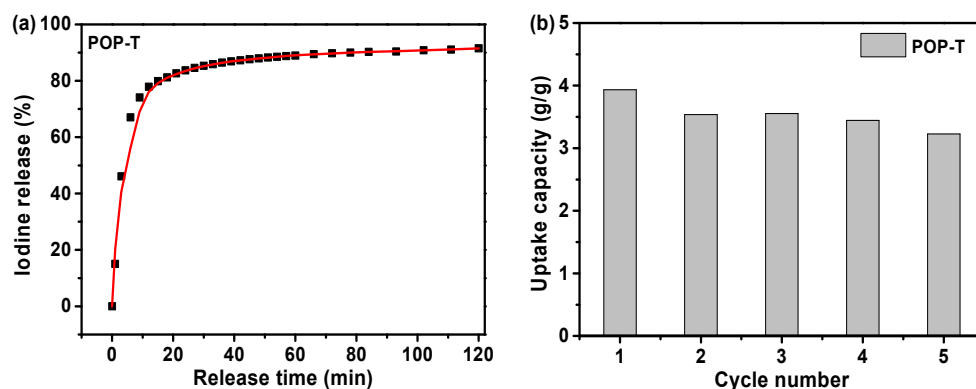
Figure 5. (**a**) The iodine released from I_2@POP-T into methanol, (**b**) Cyclic stability of POP-T.

In addition, we investigated the iodine adsorption capacity of POP-E, POP-T and POP-P in a solution environment. The adsorption experiment of iodine was carried out in n-hexane (details are given in Sections S3 and S6 in the Supplementary Materials). The experimental results showed that all three POPs exhibited good iodine removal rates in n-hexane solution at different concentrations. Their iodine uptake capabilities were 199.7, 193.4 and 150.7 mg·g^{-1} for POP-E, POP-T and POP-P, respectively, when the concentration of iodine in n-hexane was 100 mg·L^{-1}. The values were 546.1, 594.0 and 489.7 mg·g^{-1} and 610.5, 902.8 and 682.3 mg·L^{-1} when the concentration of iodine in n-hexane was 300 and 500 mg·L^{-1}, respectively (Figure 6a). The removal efficiencies of POP-E, POP-T and POP-P were 99.9%, 96.7% and 75.3% in 100 mg·L^{-1} iodine-n-hexane solution: 91.0%, 99.0% and 81.6% in 300 mg·L^{-1} iodine-n-hexane solution and 61.1%, 90.3% and 68.2% in 500 mg·L^{-1} iodine-n-hexane solution, respectively (Figure 6b). Obviously, POP-T has the best iodine adsorption capacity in n-hexane among the three POPs, which is consistent with the adsorption performance of iodine vapor (Figure 6). The iodine adsorption curves of three POPs were determined in 300 mg·L^{-1} iodine-n-hexane solution monitored by UV/ Vis spectra (Figure S17). Due to the effect of solvent encapsulation, the adsorption capacity of POPs in iodine solution was lower than their adsorption capacity for iodine vapor.
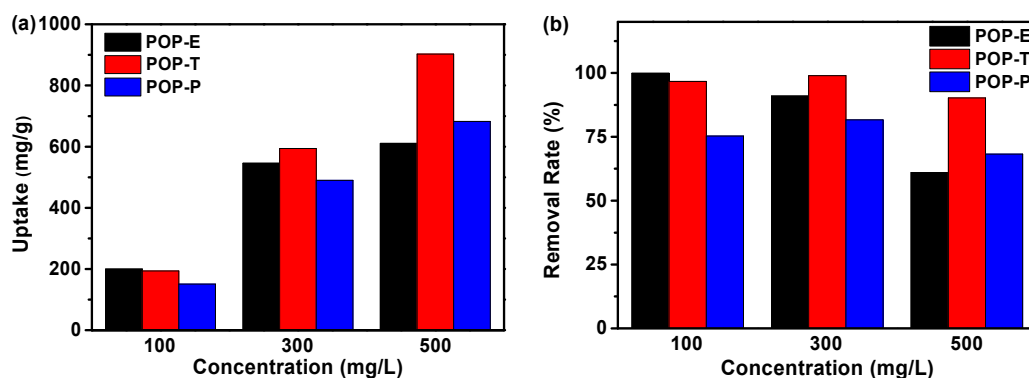
Figure 6. (**a**) Iodine uptake performance of POP-E, POP-T and POP-P in n-hexane solution. (**b**) Removal rate of POP-E, POP-T and POP-P for iodine in n-hexane solution.

3. Conclusions

In summary, three kinds of electron-rich porous organic polymers have been successfully constructed via a Schiff base reaction. The large π-π conjugated system between

aromatic rings in the three POPs formed charge-transfer complexes with adsorbed iodine molecules, which afforded the POPs with strong iodine adsorption capacity. Although the three POPs feature low specific surface area and pore volume, they all showed good iodine adsorption capacity, which indicated that specific surface area and pore volume are not the prerequisite to determine the iodine adsorption performance of POPs. Furthermore, our results revealed that the iodine adsorption capacity of POPs can be enhanced by introducing electron-rich units into the framework of POPs, and this effect could be further enhanced by introducing heteroatoms into the electron-rich structure. The three POPs not only showed good iodine vapor adsorption capacity, but also exhibited great iodine removal performance in iodine-n-hexane solution. We envision that these results might open a novel way to design porous materials for efficient iodine as well as other pollutant capture.

Supplementary Materials: The following supporting information can be downloaded at: https://www.mdpi.com/article/10.3390/molecules27165161/s1, Figure S1: Scheme for the synthesis of TFPA monomer; Figure S2: ^{1}H NMR spectrum of TFPA; Figure S3: Scheme for the synthesis of TAPE monomer; Figure S4: ^{1}H NMR spectrum of TNPE; Figure S5: ^{1}H NMR spectrum of TAPE; Figure S6: Scheme for the synthesis of PyTTA monomer; Figure S7: ^{1}H NMR spectrum of PyTTA; Figure S8: PXRD spectra of POP-E, POP-T and POP-P; Figure S9: TGA curves of POP-E, POP-T and POP-P; Figure S10: SEM images of (a,b) for POP-E; (c,d) for POP-T; (e,f) for POP-P; Figure S11: (a) XPS spectrum of POP-T, (b) XPS spectrum of N 1s in POP-T, (c) XPS spectrum of I2@POP-T, (d) XPS spectrum of N 1s in I2@POP-T; Figure S12: TGA curves of POP-T and I2@POP-T; Figure S13: Working curve for iodine in methanol solution obtained from UV-Vis spectroscopy absorbed at 226 nm; Figure S14: UV-vis spectra for I2@POP-T (0.1 mg) released from methanol solution (3 mL) at different times; Figure S15: Working curve for iodine n-hexane solution with various concentrations obtained from UV-vis spectroscopy absorbed at 523 nm; Figure S16: UV-vis spectra for POP-E, POP-T and POP-P (5.0 mg) at different concentrations of iodine in n-hexane solution (100 mg·L^{-1}, 300 mg·L^{-1} and 500 mg·L^{-1}, 10 mL) after the POPs were adsorbed under dark conditions for 72 h; Figure S17: (a,c,e) UV-vis spectra for POP-E, POP-T and POP-P (5.0 mg) in 300 mg·L^{-1} of iodine in n-hexane solution (10 mL) at different times. (b,d,f) Fitting curves of adsorption of POP-E, POP-T and POP-P in 300 mg·L^{-1} iodine in n-hexane solution; Table S1: Summary of representatively reported adsorbents with our work for iodine vapor adsorption under ambient pressure; References citation of [55–78].

Author Contributions: Conceptualization, X.S. and Y.G.; methodology, P.T. and J.Q.; software, H.H.; validation, P.T., Z.A. and M.W.; formal analysis, P.T. and Y.L.; investigation, X.G., H.X. and F.L.; resources, X.S., H.X. and Y.G.; data curation, P.T. and Z.A.; writing—original draft preparation, P.T.; writing—review and editing, S.X. and Y.G.; visualization, Y.G.; supervision, Y.G.; project administration, Y.G.; funding acquisition, X.S., H.X. and Y.G. All authors have read and agreed to the published version of the manuscript.

Institutional Review Board Statement: Not applicable.

Informed Consent Statement: Not applicable.

Data Availability Statement: Not applicable.

Conflicts of Interest: The authors declare no conflict of interest.

References

1. De Rooij, D.G.; van de Kant, H.J.G.; Dol, R.; Wagemaker, G.; van Buul, P.P.W.; van Duijn-Goedhart, A.; de Jong, F.H.; Broerse, J.J. Long-Term Effects of Irradiation Before Adulthood on Reproductive Function in the Male Rhesus Monkey1. *Biol. Reprod.* **2002**, *66*, 486–494. [CrossRef] [PubMed]
2. Ogilvy-Stuart, A.L.; Shalet, S.M. Effect of Radiation on the Human Reproductive System. *Environ. Health Perspect.* **1993**, *101*, 109–116. [PubMed]

3. Ten Hoeve, J.E.; Jacobson, M.Z. Worldwide health effects of the Fukushima Daiichi nuclear accident. *Energy Environ. Sci.* **2012**, *5*, 8743–8757. [CrossRef]

4. Saiz-Lopez, A.; Plane, J.M.C.; Baker, A.R.; Carpenter, L.J.; von Glasow, R.; Martin, J.C.G.; McFiggans, G.; Saunders, R.W. Atmospheric Chemistry of Iodine. *Chem. Rev.* **2012**, *112*, 1773–1804. [CrossRef]

5. Qian, X.; Zhu, Z.-Q.; Sun, H.-X.; Ren, F.; Mu, P.; Liang, W.; Chen, L.; Li, A. Capture and Reversible Storage of Volatile Iodine by Novel Conjugated Microporous Polymers Containing Thiophene Units. *ACS Appl. Mater. Interfaces* **2016**, *8*, 21063–21069. [CrossRef]

6. Sun, H.; Yang, B.; Li, A. Biomass derived porous carbon for efficient capture of carbon dioxide, organic contaminants and volatile iodine with exceptionally high uptake. *Chem. Eng. J.* **2019**, *372*, 65–73. [CrossRef]

7. Deitz, V.R. Interaction of radioactive iodine gaseous species with nuclear-grade activated carbons. *Carbon* **1987**, *25*, 31–38. [CrossRef]

8. Zhou, J.; Lan, T.; Li, T.; Chen, Q.; Bai, P.; Liu, F.; Yuan, Z.; Zheng, W.; Luo, X.; Yan, W.; et al. Highly efficient capture of iodine in spent fuel reprocessing off-gas by novelly porous copper-doped silica zeolites. *Sep. Purif. Technol.* **2022**, *290*, 120895. [CrossRef]

9. Riley, B.J.; Chong, S.; Schmid, J.; Marcial, J.; Nienhuis, E.T.; Bera, M.K.; Lee, S.; Canfield, N.L.; Kim, S.; Derewinski, M.A.; et al. Role of Zeolite Structural Properties toward Iodine Capture: A Head-to-head Evaluation of Framework Type and Chemical Composition. *ACS Appl. Mater. Interfaces* **2022**, *14*, 18439–18452. [CrossRef]

10. Tung Cao Thanh, P.; Docao, S.; Hwang, I.C.; Song, M.K.; Choi, D.Y.; Moon, D.; Oleynikov, P.; Yoon, K.B. Capture of iodine and organic iodides using silica zeolites and the semiconductor behaviour of iodine in a silica zeolite. *Energy Environ. Sci.* **2016**, *9*, 1050–1062.

11. Asmussen, R.M.; Matyas, J.; Qafoku, N.P.; Kruger, A.A. Silver-functionalized silica aerogels and their application in the removal of iodine from aqueous environments. *J. Hazard. Mater.* **2019**, *379*, 119364. [CrossRef] [PubMed]

12. Matyas, J.; Ilton, E.S.; Kovarik, L. Silver-functionalized silica aerogel: Towards an understanding of aging on iodine sorption performance. *RSC Adv.* **2018**, *8*, 31843–31852. [CrossRef] [PubMed]

13. Shen, Z.; Wiechert, A.I.; Choi, S.; Ladshaw, A.P.; Tavlarides, L.L.; Tsouris, C.; Yiacoumi, S. Silver-functionalized silica aerogel for iodine capture: Adsorbent aging by NO_2 in spent nuclear fuel reprocessing off-gas. *Microporous Mesoporous Mater.* **2022**, *336*, 111898. [CrossRef]

14. Zhang, X.; Maddock, J.; Nenoff, T.M.; Denecke, M.A.; Yang, S.; Schröder, M. Adsorption of iodine in metal–organic framework materials. *Chem. Soc. Rev.* **2022**, *51*, 3243–3262. [CrossRef] [PubMed]

15. Schaefer, T.C.; Becker, J.; Seuffert, M.T.; Heuler, D.; Sedykh, A.E.; Mueller-Buschbaum, K. Iodine Chemisorption, Interpenetration and Polycatenation: Cationic MOFs and CPs from Group 13 Metal Halides and Dipyridyl Linkers. *Chem. Eur. J.* **2022**, *28*, e2021041. [CrossRef] [PubMed]

16. Wang, L.; Li, T.; Dong, X.; Pang, M.; Xiao, S.; Zhang, W. Thiophene-based MOFs for iodine capture: Effect of pore structures and interaction mechanism. *Chem. Eng. J.* **2021**, *425*, 130578. [CrossRef]

17. Xie, W.; Cui, D.; Zhang, S.-R.; Xu, Y.-H.; Jiang, D.-L. Iodine capture in porous organic polymers and metal-organic frameworks materials. *Mater. Horizons* **2019**, *6*, 1571–1595. [CrossRef]

18. Xu, M.; Wang, T.; Zhou, L.; Hua, D. Fluorescent conjugated mesoporous polymers with N,N-diethylpropylamine for the efficient capture and real-time detection of volatile iodine. *J. Mater. Chem. A* **2020**, *8*, 1966–1974. [CrossRef]

19. Zhang, Y.; Yi, D.; Tu, P.; Yang, S.; Xie, Q.; Gao, Z.; Wu, S.; Yu, G. Boosting radioactive iodine capture of microporous polymers through strengthened host-guest interaction. *Microporous Mesoporous Mater.* **2021**, *321*, 111148. [CrossRef]

20. Geng, T.; Chen, G.; Ma, L.; Zhang, C.; Zhang, W.; Xu, H. The spirobifluorene-based fluorescent conjugated microporous polymers for reversible adsorbing iodine, fluorescent sensing iodine and nitroaromatic compounds. *Euro. Polym. J.* **2019**, *115*, 37–44. [CrossRef]

21. Geng, T.; Ma, L.; Chen, G.; Zhang, C.; Zhang, W.; Niu, Q. Fluorescent conjugated microporous polymers containing pyrazine moieties for adsorbing and fluorescent sensing of iodine. *Environ. Sci. Pollut. Res.* **2020**, *27*, 20235–20245. [CrossRef] [PubMed]

22. Du, W.; Qin, Y.; Ni, C.; Dai, W.; Zou, J. Efficient Capture of Volatile Iodine by Thiophene-Containing Porous Organic Polymers. *ACS Appl. Polym.* **2020**, *2*, 5121–5128. [CrossRef]

23. Yan, Z.; Yuan, Y.; Tian, Y.; Zhang, D.; Zhu, G. Highly Efficient Enrichment of Volatile Iodine by Charged Porous Aromatic Frameworks with Three Sorption Sites. *Angew. Chem. Int. Ed.* **2015**, *54*, 12733–12737. [CrossRef] [PubMed]

24. Wang, J.; Wang, C.; Wang, H.; Jin, B.; Zhang, P.; Li, L.; Miao, S. Synthesis of N-containing porous aromatic frameworks via Scholl reaction for reversible iodine capture. *Microporous Mesoporous Mater.* **2021**, *310*, 110596. [CrossRef]

25. Li, B.; Zhang, Y.; Krishna, R.; Yao, K.; Han, Y.; Wu, Z.; Ma, D.; Shi, Z.; Pham, T.; Space, B.; et al. Introduction of π-Complexation into Porous Aromatic Framework for Highly Selective Adsorption of Ethylene over Ethane. *J. Am. Chem. Soc.* **2014**, *136*, 8654–8660. [CrossRef]

26. Wu, X.; Shaibani, M.; Smith, S.J.D.; Konstas, K.; Hill, M.R.; Wang, H.; Zhang, K.; Xie, Z. Microporous carbon from fullerene impregnated porous aromatic frameworks for improving the desalination performance of thin film composite forward osmosis membranes. *J. Mater. Chem. A* **2018**, *6*, 11327–11336. [CrossRef]

27. Li, X.; Chen, G.; Jia, Q. One-pot synthesis of viologen-based hypercrosslinked polymers for efficient volatile iodine capture. *Microporous Mesoporous Mater.* **2019**, *279*, 186–192. [CrossRef]

28. Li, X.; Chen, G.; Jia, Q. Highly efficient iodine capture by task-specific polyethylenimine impregnated hypercrosslinked polymers. *J. Taiwan Inst. Chem. Eng.* **2018**, *93*, 660–666. [CrossRef]

29. Li, X.; Chen, G.; Ma, J.; Jia, Q. Pyrrolidinone-based hypercrosslinked polymers for reversible capture of radioactive iodine. *Sep. Purif. Technol.* **2019**, *210*, 995–1000. [CrossRef]

30. Tu, P.; He, X.; Abu-Reziq, R.; Pan, C.; Tang, J.; Yu, G. Fluorinated covalent triazine frameworks for effective CH_4 separation and iodine vapor uptake. *Sep. Purif. Technol.* **2022**, *290*, 120857. [CrossRef]

31. Chang, S.; Xie, W.; Yao, C.; Xu, G.; Zhang, S.; Xu, Y. Preparation of covalent triazine frameworks with multiactive sites for efficient and reversible iodine capture. *Eur. Polym. J.* **2021**, *159*, 110753. [CrossRef]

32. Jiang, Q.; Huang, H.; Tang, Y.; Zhang, Y.; Zhong, C. Highly Porous Covalent Triazine Frameworks for Reversible Iodine Capture and Efficient Removal of Dye. *Ind. Eng. Chem. Res.* **2018**, *57*, 15114–15121. [CrossRef]

33. Geng, T.-M.; Fang, X.-C.; Wang, F.-Q.; Zhu, F. The Synthesis of Covalent Triazine-Based Frameworks via Friedel–Crafts Reactions of Cyanuric Chloride with Thienyl and Carbazolyl Derivatives for Fluorescence Sensing to Picric Acid, Iodine and Capturing Iodine. *Macromol. Mater. Eng.* **2021**, *306*, 2100461. [CrossRef]

34. An, S.; Zhu, X.; He, Y.; Yang, L.; Wang, H.; Jin, S.; Hu, J.; Liu, H. Porosity Modulation in Two-Dimensional Covalent Organic Frameworks Leads to Enhanced Iodine Adsorption Performance. *Ind. Eng. Chem. Res.* **2019**, *58*, 10495–10502. [CrossRef]

35. Xie, Y.; Pan, T.; Lei, Q.; Chen, C.; Dong, X.; Yuan, Y.; Shen, J.; Cai, Y.; Zhou, C.; Pinnau, I.; et al. Ionic Functionalization of Multivariate Covalent Organic Frameworks to Achieve an Exceptionally High Iodine-Capture Capacity. *Angew. Chem. Int. Ed.* **2021**, *60*, 22432–22440. [CrossRef] [PubMed]

36. Wen, Z.; Wang, S.; Fu, S.; Qian, J.; Yan, Q.; Xu, H.; Zuo, K.; Su, X.; Zeng, C.; Gao, Y. A Two-dimensional Dual-pore Covalent Organic Framework for Efficient Iodine Capture. *Chem. Res. Chin. Univ.* **2022**, *38*, 472–477. [CrossRef]

37. Wang, C.; Wang, Y.; Ge, R.; Song, X.; Xing, X.; Jiang, Q.; Lu, H.; Hao, C.; Guo, X.; Gao, Y.; et al. A 3D Covalent Organic Framework with Exceptionally High Iodine Capture Capability. *Chem. Eur. J.* **2018**, *24*, 585–589. [CrossRef]

38. Chang, J.; Li, H.; Zhao, J.; Guan, X.; Li, C.; Yu, G.; Valtchev, V.; Yan, Y.; Qiu, S.; Fang, Q. Tetrathiafulvalene-based covalent organic frameworks for ultrahigh iodine capture. *Chem. Sci.* **2021**, *12*, 8452–8457. [CrossRef]

39. Song, S.; Shi, Y.; Liu, N.; Liu, F. Theoretical Screening and Experimental Synthesis of Ultrahigh-Iodine Capture Covalent Organic Frameworks. *ACS Appl. Mater. Interfaces* **2021**, *13*, 10513–10523. [CrossRef]

40. Sprick, R.S.; Jiang, J.X.; Bonillo, B.; Ren, S.; Ratvijitvech, T.; Guiglion, P.; Zwijnenburg, M.A.; Adams, D.J.; Cooper, A.I. Tunable Organic Photocatalysts for Visible-Light-Driven Hydrogen Evolution. *J. Am. Chem. Soc.* **2015**, *137*, 3265–3270. [CrossRef]

41. Li, L.; Cai, Z.; Wu, Q.; Lo, W.Y.; Zhang, N.; Chen, L.X.; Yu, L. Rational Design of Porous Conjugated Polymers and Roles of Residual Palladium for Photocatalytic Hydrogen Production. *J. Am. Chem. Soc.* **2016**, *138*, 7681–7686. [CrossRef] [PubMed]

42. Sun, L.; Liang, Z.; Yu, J.; Xu, R. Luminescent microporous organic polymers containing the 1,3,5-tri(4-ethenylphenyl)benzene unit constructed by Heck coupling reaction. *Polym. Chem.* **2013**, *4*, 1932–1938. [CrossRef]

43. Zhang, K.; Kopetzki, D.; Seeberger, P.H.; Antonietti, M.; Vilela, F. Surface Area Control and Photocatalytic Activity of Conjugated Microporous Poly(benzothiadiazole) Networks. *Angew. Chem. Int. Ed.* **2013**, *52*, 1432–1436. [CrossRef] [PubMed]

44. Zhao, Y.; Liu, H.; Wu, C.; Zhang, Z.; Pan, Q.; Hu, F.; Wang, R.; Li, P.; Huang, X.; Li, Z. Fully Conjugated Two-Dimensional sp2-Carbon Covalent Organic Frameworks as Artificial Photosystem I with High Efficiency. *Angew. Chem. Int. Ed.* **2019**, *58*, 5376–5381. [CrossRef]

45. Schmidt, J.; Werner, M.; Thomas, A. Conjugated Microporous Polymer Networks via Yamamoto Polymerization. *Macromolecules* **2009**, *42*, 4426–4429. [CrossRef]

46. Wang, L.; Wan, Y.; Ding, Y.; Wu, S.; Zhang, Y.; Zhang, X.; Zhang, G.; Xiong, Y.; Wu, X.; Yang, J.; et al. Conjugated Microporous Polymer Nanosheets for Overall Water Splitting Using Visible Light. *Adv. Mater.* **2017**, *29*, 1702428. [CrossRef]

47. Li, L.; Deng, J.; Guo, J.; Yue, H. Synthesis and properties of microporous organic polymers based on adamantane. *Prog. Chem.* **2020**, *32*, 190–203.

48. Falaise, C.; Volkringer, C.; Facqueur, J.; Bousquet, T.; Gasnot, L.; Loiseau, T. Capture of iodine in highly stable metal–organic frameworks: A systematic study. *Chem. Commun.* **2013**, *49*, 10320–10322. [CrossRef]

49. Guo, Z.; Sun, P.; Zhang, X.; Lin, J.; Shi, T.; Liu, S.; Sun, A.; Li, Z. Amorphous Porous Organic Polymers Based on Schiff-Base Chemistry for Highly Efficient Iodine Capture. *Chem. Asian J.* **2018**, *13*, 2046–2053. [CrossRef]

50. Song, S.; Shi, Y.; Liu, N.; Liu, F. C=N linked covalent organic framework for the efficient adsorption of iodine in vapor and solution. *RSC Adv.* **2021**, *11*, 10512–10523. [CrossRef]

51. Xia, M. Study on Gases and Iodine Adsorption of Microporous Organic Polymers. Master's Thesis, Dalian University of Technology, Dalian, China, June 2019.

52. Li, J.; Zhang, H.; Zhang, L.; Wang, K.; Wang, Z.; Liu, G.; Zhao, Y.; Zeng, Y. Two-dimensional covalent–organic frameworks for ultrahigh iodine capture. *J. Mater. Chem. A* **2020**, *8*, 9523–9527. [CrossRef]

53. Hsu, S.L.; Signorelli, A.J.; Pez, G.P.; Baughman, H. Highly conducting iodine derivatives of polyacetylene: Raman, XPS and x-ray diffraction studies. *J. Chem. Phys.* **1978**, *69*, 106–111. [CrossRef]

54. Cambedouzou, J.; Sauvajol, J.L.; Rahmani, A.; Flahaut, E.; Peigney, A.; Laurent, C. Raman spectroscopy of iodine-doped double-walled carbon nanotubes. *Phys. Rev. B* **2004**, *69*, 235422. [CrossRef]

55. Plietzsch, O.; Schilling, C.I.; Tolev, M.; Nieger, M.; Richert, C.; Muller, T.; Bräse, S. Four-fold click reactions: Generation of tetrahedral methane- and adamantane-based building blocks for higher-order molecular assemblies. *Org. Biomol. Chem.* **2009**, *7*, 4734–4743. [CrossRef] [PubMed]

56. Li, G.; Zhang, B.; Yan, J.; Wang, Z. Micro- and mesoporous poly(Schiff-base)s constructed from different building blocks and their adsorption behaviors towards organic vapors and CO_2 gas. *J. Mater. Chem. A* **2014**, *2*, 18881–18888. [CrossRef]

57. Lu, J.; Zhang, J. Facile synthesis of azo-linked porous organic frameworks via reductive homocoupling for selective CO_2 capture. *J. Mater. Chem. A* **2014**, *2*, 13831–13834. [CrossRef]

58. Ascherl, L.; Evans, E.W.; Gorman, J.; Orsborne, S.; Bessinger, D.; Bein, T.; Friend, R.H.; Auras, F. Perylene-Based Covalent Organic Frameworks for Acid Vapor Sensing. *J. Am. Chem. Soc.* **2019**, *141*, 15693–15699. [CrossRef]

59. Wang, P.; Xu, Q.; Li, Z.; Jiang, W.; Jiang, Q.; Jiang, D. Exceptional Iodine Capture in 2D Covalent Organic Frameworks. *Adv. Mater.* **2018**, *30*, 1801991. [CrossRef]

60. Guo, X.; Tian, Y.; Zhang, M.; Li, Y.; Wen, R.; Li, X.; Li, X.; Xue, Y.; Ma, L.; Xia, C.; et al. Mechanistic Insight into Hydrogen-Bond-Controlled Crystallinity and Adsorption Property of Covalent Organic Frameworks from Flexible Building Blocks. *Chem. Mater.* **2018**, *30*, 2299–2308. [CrossRef]

61. Yin, Z.-J.; Xu, S.-Q.; Zhan, T.-G.; Qi, Q.-Y.; Wu, Z.-Q.; Zhao, X. Ultrahigh volatile iodine uptake by hollow microspheres formed from a heteropore covalent organic framework. *Chem. Commun.* **2017**, *53*, 7266–7269. [CrossRef]

62. Qian, X.; Wang, B.; Zhu, Z.-Q.; Sun, H.-X.; Ren, F.; Mu, P.; Ma, C.; Liang, W.-D.; Li, A. Novel N-rich porous organic polymers with extremely high uptake for capture and reversible storage of volatile iodine. *J. Hazard. Mater.* **2017**, *338*, 224–232. [CrossRef] [PubMed]

63. Ren, F.; Zhu, Z.; Qian, X.; Liang, W.; Mu, P.; Sun, H.; Liu, J.; Li, A. Novel thiophene-bearing conjugated microporous polymer honeycomb-like porous spheres with ultrahigh iodine uptake. *Chem. Commun.* **2016**, *52*, 9797–9800. [CrossRef] [PubMed]

64. Liao, Y.; Weber, J.; Mills, B.M.; Ren, Z.; Faul, C.F.J. Highly Efficient and Reversible Iodine Capture in Hexaphenylbenzene-Based Conjugated Microporous Polymers. *Macromolecules* **2016**, *49*, 6322–6333. [CrossRef]

65. Shetty, D.; Raya, J.; Han, D.S.; Asfari, Z.; Olsen, J.-C.; Trabolsi, A. Lithiated Polycalix[4]arenes for Efficient Adsorption of Iodine from Solution and Vapor Phases. *Chem. Mater.* **2017**, *29*, 8968–8972. [CrossRef]

66. Li, H.; Ding, X.; Han, B.-H. Porous Azo-Bridged Porphyrin–Phthalocyanine Network with High Iodine Capture Capability. *Chem. A Eur. J.* **2016**, *22*, 11863–11868. [CrossRef] [PubMed]

67. Zhu, Y.; Ji, Y.-J.; Wang, D.-G.; Zhang, Y.; Tang, H.; Jia, X.-R.; Song, M.; Yu, G.; Kuang, G.-C. BODIPY-based conjugated porous polymers for highly efficient volatile iodine capture. *J. Mater. Chem. A* **2017**, *5*, 6622–6629. [CrossRef]

68. Weng, J.-Y.; Xu, Y.-L.; Song, W.-C.; Zhang, Y.-H. Tuning the adsorption and fluorescence properties of aminal-linked porous organic polymers through N-heterocyclic group decoration. *J. Polym. Sci. Part A Polym. Chem.* **2016**, *54*, 1724. [CrossRef]

69. Dang, Q.-Q.; Wang, X.-M.; Zhan, Y.-F.; Zhang, X.-M. An azo-linked porous triptycene network as an absorbent for CO_2 and iodine uptake. *Polym. Chem.* **2016**, *7*, 643–647. [CrossRef]

70. Chen, Y.; Sun, H.; Yang, R.; Wang, T.; Pei, C.; Xiang, Z.; Zhu, Z.; Liang, W.; Li, A.; Deng, W. Synthesis of conjugated microporous polymer nanotubes with large surface areas as absorbents for iodine and CO_2 uptake. *J. Mater. Chem. A* **2015**, *3*, 87–91. [CrossRef]

71. Sigen, A.; Zhang, Y.; Li, Z.; Xia, H.; Xue, M.; Liu, X.; Mu, Y. Highly efficient and reversible iodine capture using a metalloporphyrin-based conjugated microporous polymer. *Chem. Commun.* **2014**, *50*, 8495–8498.

72. Pei, C.; Ben, T.; Xu, S.; Qiu, S. Ultrahigh iodine adsorption in porous organic frameworks. *J. Mater. Chem. A* **2014**, *2*, 7179–7187. [CrossRef]

73. Ma, H.; Chen, J.-J.; Tan, L.; Bu, J.-H.; Zhu, Y.; Tan, B.; Zhang, C. Nitrogen-Rich Triptycene-Based Porous Polymer for Gas Storage and Iodine Enrichment. *ACS Macro Lett.* **2016**, *5*, 1039–1043. [CrossRef] [PubMed]

74. Mu, P.; Sun, H.; Chen, T.; Zhang, W.; Zhu, Z.; Liang, W.; Li, A. A Sponge-Like 3D-PPy Monolithic Material for Reversible Adsorption of Radioactive Iodine. *Macromol. Mater. Eng.* **2017**, *302*, 1700156. [CrossRef]

75. Park, K.C.; Cho, J.; Lee, C.Y. Porphyrin and pyrene-based conjugated microporous polymer for efficient sequestration of CO_2 and iodine and photosensitization for singlet oxygen generation. *RSC Adv.* **2016**, *6*, 75478–75481. [CrossRef]

76. Das, G.; Skorjanc, T.; Sharma, S.K.; Prakasam, T.; Platas-Iglesias, C.; Han, D.S.; Raya, J.; Olsen, J.-C.; Jagannathan, R.; Trabolsi, A. Morphological Diversity in Nanoporous Covalent Organic Materials Derived from Viologen and Pyrene. *Chemnanomat* **2018**, *4*, 61–65. [CrossRef]

77. Li, L.; Chen, R.; Li, Y.; Xiong, T.; Li, Y. Novel cotton fiber-covalent organic framework hybrid monolith for reversible capture of iodine. *Cellulose* **2020**, *27*, 5879–5892. [CrossRef]

78. Li, Y.; Li, Y.; Zhao, Q.; Li, L.; Chen, R.; He, C. Cotton fiber functionalized with 2D covalent organic frameworks for iodine capture. *Cellulose* **2020**, *27*, 1517–1529. [CrossRef]